

Article

Effect of High Pressure and Temperature on the Evolution of Si Phase and Eutectic Spacing in Al-20Si Alloys

Rong Zhang, Chunming Zou, Zunjie Wei *  and Hongwei Wang *

School of Materials Science and Engineering, Harbin Institute of Technology, Harbin 150001, China; zhang_r1992@163.com (R.Z.); zouchunming1977@163.com (C.Z.)

* Correspondence: weizj@hit.edu.cn (Z.W.); wanghw@hit.edu.cn (H.W.)

Abstract: The microstructure of the Si phase in Al-20Si alloys solidified under high pressure was investigated. The results demonstrate that the morphology of Si phase transformed (bulk→short rod→long needle) with the increase of superheat temperature under high pressure. At a pressure of 3 GPa and a superheat temperature of 100 K, a microstructure with a uniform distribution of fine Si phases on the α -Al matrix was obtained in the Al-20Si alloy. In addition, a mathematical model was developed to analyze the spacing variation of the lamellar Al-Si eutectics under the effect of pressure. The lamellar Al-Si eutectics appeared at 2 GPa and superheat temperatures of 70–150 K, and at 3 GPa and superheat temperatures of 140–200 K. With the increase of pressure from 2 GPa to 3 GPa, the average spacing of lamellar Al-Si eutectics decreased from 1.2–1.6 μm to 0.9–1.1 μm . In binary alloys, the effect of pressure on the eutectic spacing is related to the volume change of the solute phase from liquid to solid. When the volume change of the solute phase from liquid to solid is negative, the lamellar eutectic spacing decreases with increasing pressure. When it is positive, the eutectic spacing increases with increasing pressure.



Citation: Zhang, R.; Zou, C.; Wei, Z.; Wang, H. Effect of High Pressure and Temperature on the Evolution of Si Phase and Eutectic Spacing in Al-20Si Alloys. *Crystals* **2021**, *11*, 705. <https://doi.org/10.3390/cryst11060705>

Academic Editor: Marek Szafranski, Simone Anzellini and Daniel Errandonea

Received: 21 May 2021
Accepted: 17 June 2021
Published: 20 June 2021

Publisher's Note: MDPI stays neutral with regard to jurisdictional claims in published maps and institutional affiliations.



Copyright: © 2021 by the authors. Licensee MDPI, Basel, Switzerland. This article is an open access article distributed under the terms and conditions of the Creative Commons Attribution (CC BY) license (<https://creativecommons.org/licenses/by/4.0/>).

Keywords: high pressure; eutectic spacing; Al-Si alloy; superheat

1. Introduction

The study of the influence of compression in the properties of metallic alloys, including morphology and microstructure, is extremely relevant for multiple technological applications [1–3]. At present, solidification phenomena are mainly described by nucleation [4–6], constitutional undercooling [7], interface stability [8–13], eutectic growth [14], dendritic growth [15,16], etc. These theories mainly consider the effects of temperature and concentration but ignore that of pressure on the solidification process. The high pressure at the GPa-level causes the microstructure of the material to be greatly refined [17–19], while at the same time, the solubility of the solute in the melt increases [20–22]. Therefore, the solidification process must take into account the effect of GPa-level pressure.

Similarly, the morphology and spacing of the eutectic can be affected by the GPa-level pressure. Temperature, pressure and composition are important variables in the study of microstructure evolution. While considering the effect of GPa-level pressure on the microstructure, the effect of temperature on the microstructure cannot be ignored. Under the combined effect of pressure and temperature, higher pressure enables the Al-20Si alloy to maintain stable interfacial morphology at higher temperatures [23]. The increase in pressure from 1 atm to 3 GPa leads to an increase in the tensile strength of the Al-20Si alloy and the refinement of the eutectic [24]. The pressure has a significant effect on the eutectics. It is necessary to study the eutectic spacing of binary alloys under the effect of high pressure.

In this paper, the Si phase in Al-20Si alloy solidified under high pressure was investigated. Then, based on the classical eutectic growth model, the mathematical model of eutectic spacing under the effect of pressure was developed. Finally, the eutectic spacing was investigated by this mathematical model.

2. Materials and Methods

Al-20Si (wt%) powders (Tian Jiu Technology, purity 99.9 %, 9–11 μm , Changsha, China) were used as the raw materials. The powders were cold-pressed under 300 MPa to obtain $\Phi 20 \times 18$ mm cylinders. Figure 1 shows the HTDS-032F high-pressure equipment. The pressure was calibrated by the I-II phase transition of Bi (at 2.55 GPa) in our previous works [25]. The temperature was calibrated by a thermocouple (B-type). The details of the cell assembly can be found in [26]. The samples were pressurized to the target pressure (2 GPa and 3 GPa), then a current was applied to the graphite heater to heat the samples to the target temperature for 5 min, and finally, the current was disconnected and cooled to room temperature at a rate of 20 K/S. The specimens were etched with 0.5 vol% hydrofluoric acid solution for 10 s or 20 min (deep-etched). The microstructure was analyzed using a scanning electron microscope (Merlin Compact, ZEISS, Germany) operated at 20 kV.

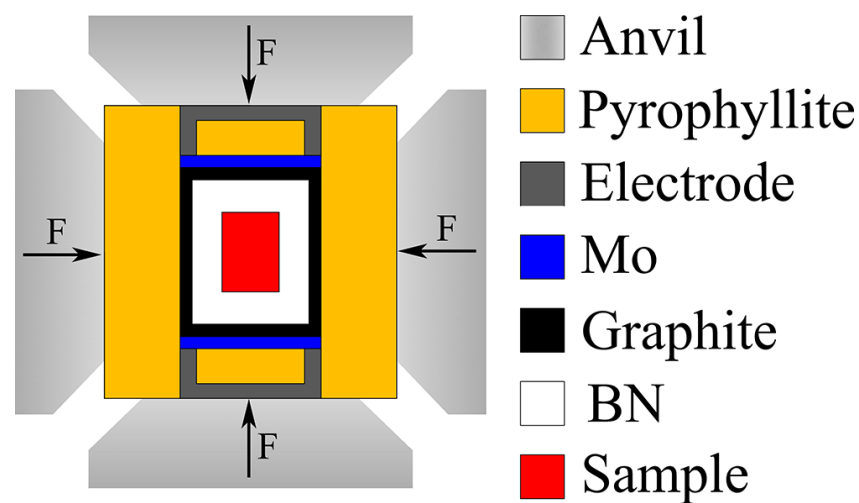


Figure 1. High-pressure experiment.

3. Results

3.1. Microstructure of Al-Si Alloys under High Pressure

Figures 2 and 3 show the microstructure morphologies of the lamellar Al-Si eutectics and anomalous Si phases under high pressure, respectively. The dark phases are the α -Al phases, while the bright phases are the Si phases. In our previous study [23], the microstructure morphologies of the α -Al phases in the high-pressure solidified Al-20Si alloy underwent a process of change from dendritic to cellular, spherical and planar as the melt superheat temperature decreased. It is clearly observed in Figure 2 that the Al-Si eutectics have lamellar microstructure morphologies when the α -Al phases grow in dendritic and cellular forms. As can be clearly observed in Figure 3, anomalous Si phases appear when the α -Al phases grow in planar and spherical forms, and the Si phases have bulk morphologies. Under high-pressure solidification conditions, changes in the superheat temperature of the melt had an effect not only on the microstructures of the α -Al phases but also on that of the Si phases. With an increase in the superheat temperature of the melt, the microstructures of the Si phases in the high-pressure solidified Al-20Si alloy changed from bulk to short rods and then to long needles.

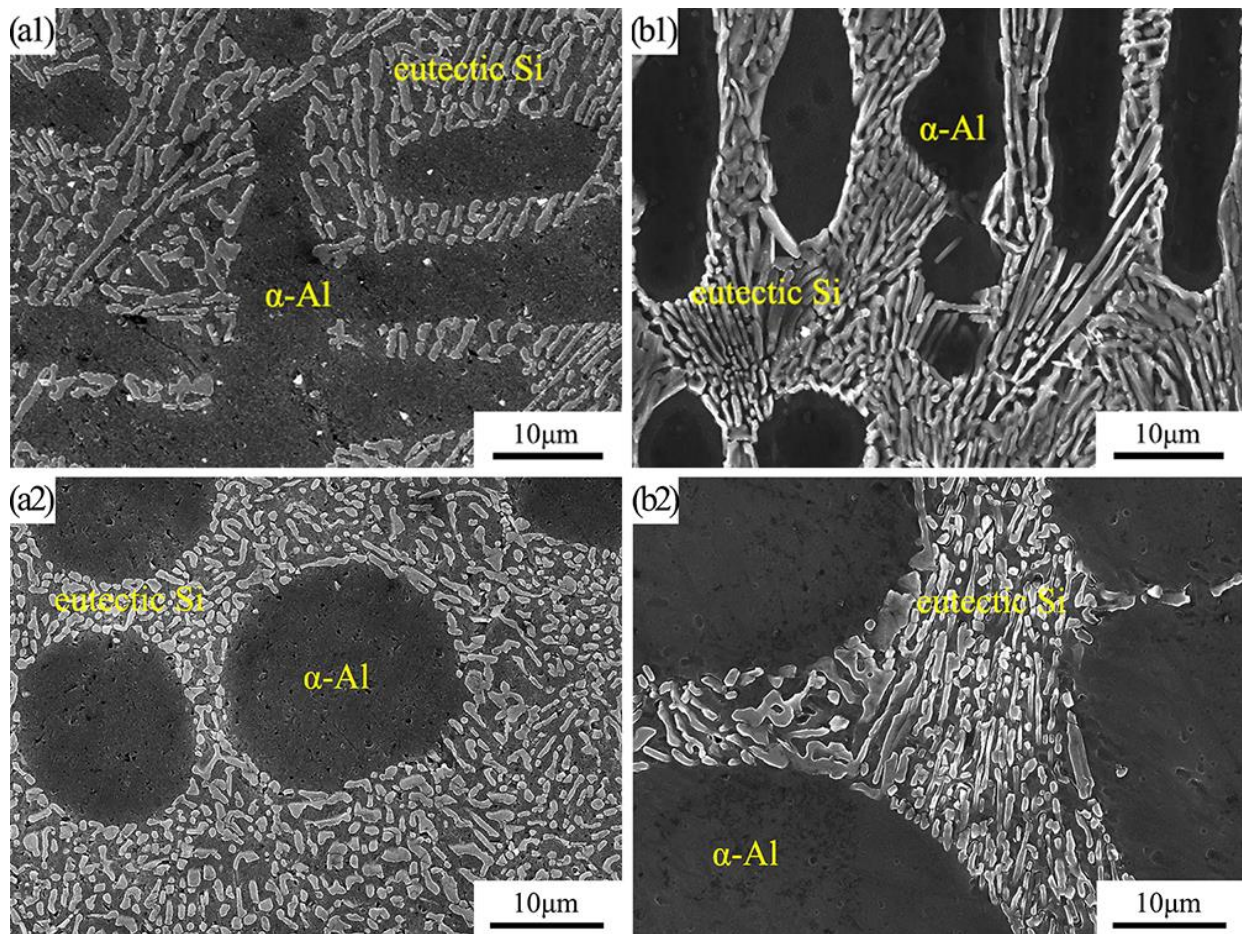


Figure 2. Microstructures of lamellar Al-Si eutectics at different pressures and superheat temperatures: (a1,a2) 2 GPa; (b1,b2) 3 GPa; (a1) 150 K; (a2) 70 K; (b1) 200 K; (b2) 140 K.

It should be noted that what appears on Figure 2 as needles and rods in fact is a section view of plates (lamella). The “aspect ratio” was defined as the ratio between the longest and shortest lines joining two points of the Si phase contour and passing through the centroid. The aspect ratios of the Si phases at different pressures and superheat temperatures are shown in Figure 4. The aspect ratios of the Si phases increased with increasing superheat temperature, corresponding to the transformation of the Si phases (bulk→short rod→long needle).

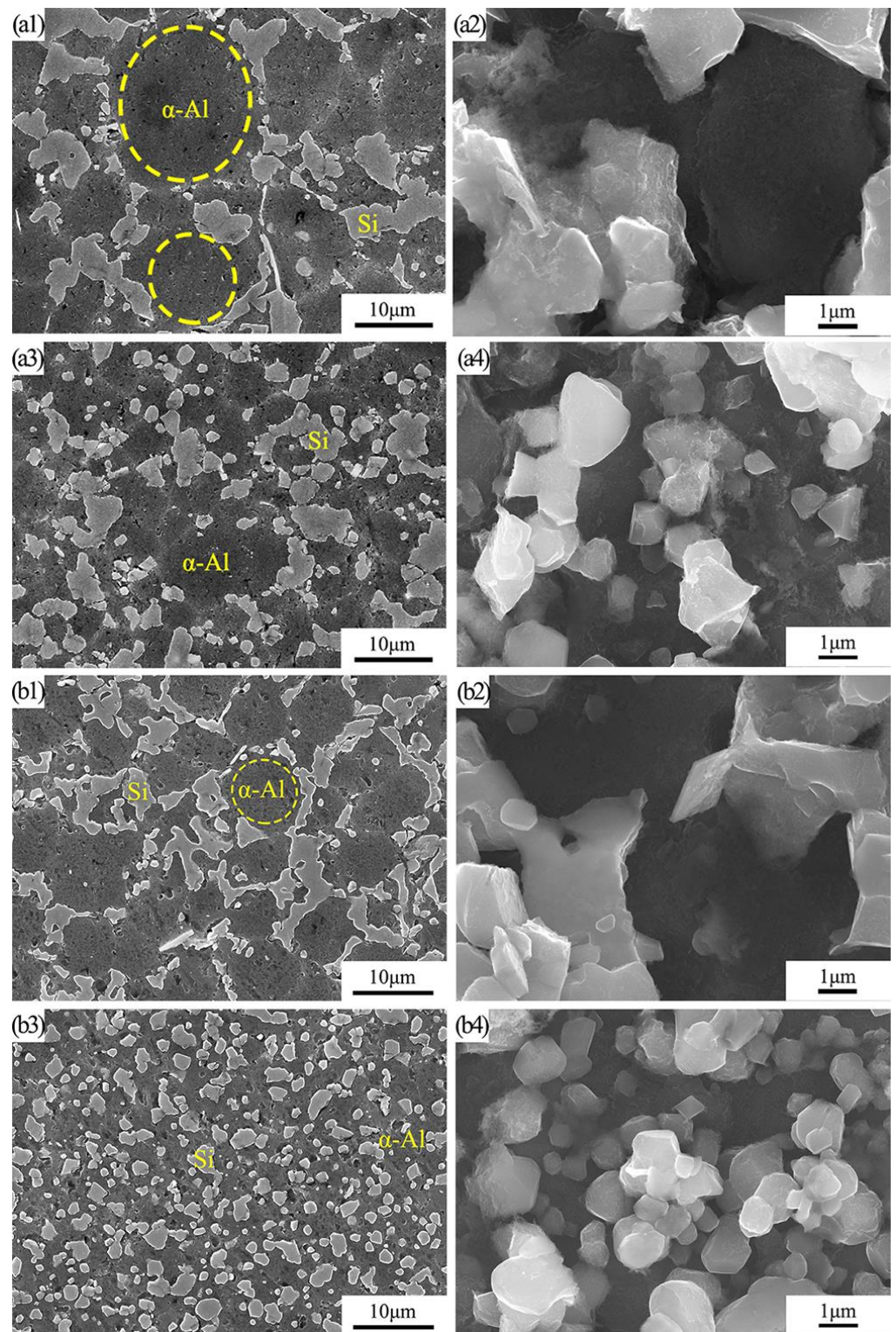


Figure 3. Microstructures of anomalous Si phases at different pressures and superheat temperatures: (a1–a4) 2 GPa; (b1–b4) 3 GPa; (a1,a2) 60 K; (a3,a4) 50 K; (b1,b2) 110 K; (b3,b4) 100 K.

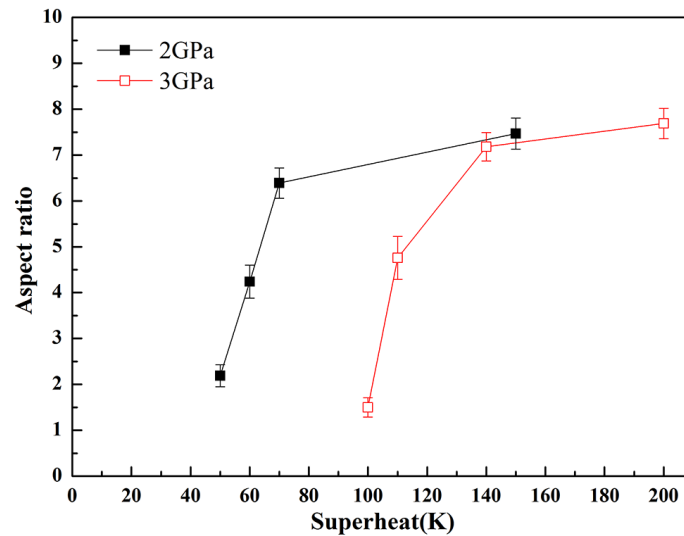


Figure 4. Aspect ratios of Si phases.

The spacing of lamellar Al-Si eutectics was measured by the random intercepts, as shown in Figure 5. Only the eutectic spacings when the Al-Si eutectics were lamellar were counted and averaged in the figure. The average eutectic spacings of the lamellar Al-Si eutectics decreased with increasing pressure.

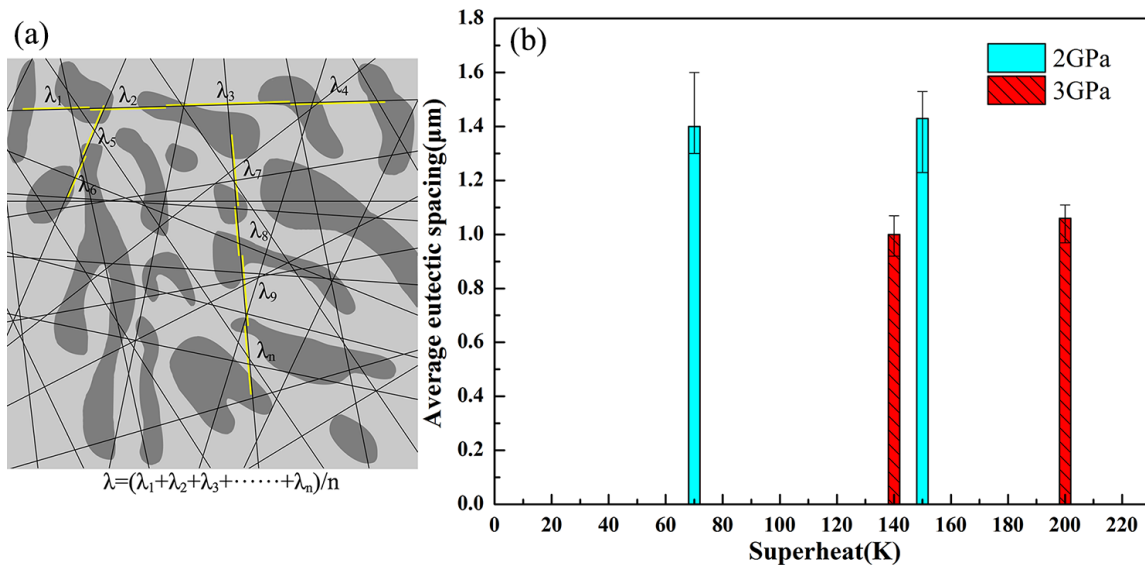


Figure 5. Average eutectic spacings of lamellar Al-Si eutectics: (a) random intercepts; (b) statistics.

It is worth mentioning that the effect of pressure on eutectic spacing should include the condition of temperature, and the two variables of pressure and temperature could not be considered independently. Based on the evolution of microstructures of Al-20Si alloy in Figures 2 and 3, it could be inferred that when the superheat temperature was 100 K, it was lamellar eutectic at 2 GPa, while it was fine Si phases at 3 GPa. It was not possible to compare the average spacings between the two.

The lamellar Al-Si eutectics appeared at 2 GPa and superheat temperatures of 70–150 K, and at 3 GPa and superheat temperatures of 140–200 K. When the Al-Si eutectics were lamellar, the spacings of the two could be compared. In the above superheat temperature range, the effect of temperature on the average eutectic spacing was small. With the increase of pressure from 2 GPa to 3 GPa, the average spacing of lamellar Al-Si eutectics decreased

from 1.2–1.6 μm to 0.9–1.1 μm . The following discussions of eutectic spacing were based on the foundation that the Al-Si eutectics were lamellar.

3.2. Morphological Evolution of the Si Phase

The increase in pressure not only increases the eutectic temperature of the Al-Si alloy, but also increases the Si content corresponding to the eutectic point [27,28]. Al-20Si alloy was actually in the hypoeutectic zone at pressures of 2 GPa and 3 GPa. The α -Al phases precipitated first, and the growth and distribution of the Si phases were influenced by the solute diffusion. The solute diffusion coefficient under high pressures can be calculated by Ref. [29]:

$$D_P = D \exp\left(-\frac{PV_0}{RT}\right) \quad (1)$$

where P (Pa) is the pressure, V_0 (m^3/mol) is the original volume of the liquid phase, $R = 8.314$ ($\text{J}/(\text{mol}\cdot\text{K})$) is the gas constant, T (K) is the temperature, D (m^2/s) is the solute diffusion coefficient in liquid. It can be seen from Equation (1) that the increase in pressure caused an exponential decrease in the solute diffusion coefficient.

When the superheat temperatures were lower, the α -Al phase grew in planar and spherical forms, while the temperature of the solid-liquid interface front increased due to the release of latent heat. Due to the lower melt temperature and exponential decrease of solute diffusion coefficient, Si atomic clusters were enriched at the solid-liquid interface front and did not have time to diffuse. When the compositional supercooling at the solid-liquid interface front reached the nucleation supercooling of the Si phase, the Si phases nucleated and grew into bulk crystals. The Si phase in the α -Al matrix was precipitated in bulk form, resulting in the disappearing of the typical lamellar eutectic and turning into an anomalous Si phase.

When the superheat temperatures were higher, the α -Al phases grew in cellular and dendritic forms. Due to the higher temperature of the melt, the Si atoms were enriched at the front of the solid-liquid interface had a certain amount of time to diffuse laterally, leading to the formation of lamellar Al-Si eutectics. The increase in pressure led to an exponential decrease in the solute diffusion coefficient, resulting in the diffusion distance of Si atoms under a pressure of 3 GPa being smaller than that of Si atoms under a pressure of 2 GPa, and thus the eutectic spacing became progressively smaller with the increase in pressure. Analyzed from the aspect of solute diffusion coefficient, the pressure had an effect on the solute diffusion coefficient, which in turn had an effect on the eutectic spacing. In addition, the increase in melt temperature led to a longer solidification time, so the morphology of the Si phase changed from bulk \rightarrow short rod \rightarrow long needle, making the aspect ratio of the Si phase increase. In fact, the lamellae of Al-Si eutectics became thinner and longer.

3.3. Effect of Pressure on Eutectic Spacing

For the lamellar eutectic growth problem, Jackson and Hunt developed a J-H mathematical model to calculate and analyze the eutectic growth process [30]. Kurz extended and simplified the theoretical expressions to predict the eutectic spacing for both the high Péclet number and the low Péclet number [13]:

$$\lambda^2 V = \frac{K_r}{K_c} \quad (2)$$

$$K_c = \frac{|m_\alpha| |m_\beta|}{|m_\alpha| + |m_\beta|} \cdot \frac{1 - K}{2\pi D} \cdot \frac{2\pi/P_c}{\left[1 + (2\pi/P_c)^2\right]^{1/2} - 1 + 2k} \quad (3)$$

$$K_r = \frac{2(1-f)|m_\beta|\Gamma_\alpha \sin \theta_\alpha + 2f|m_\alpha|\Gamma_\beta \sin \theta_\beta}{f(1-f)(|m_\alpha| + |m_\beta|)} \quad (4)$$

where λ (m) is the lamellar eutectic spacing, m_α is the liquidus slope of α phase, m_β is the liquidus slope of β phase, V (m/s) is the growth rate, P_c is the solute Péclet number, f is the volume fraction of α phase, θ ($^\circ$) is wetting angle, k is the solute distribution coefficient, Γ is the Gibbs-Thomson coefficient.

According to Kurz's theoretical derivation [13], inserting Equations (3) and (4) into Equation (2) and separating the terms related to P_c , the Equation (2) is obtained as:

$$\lambda^2 V = D\Theta \frac{(P_c^2 + 4\pi^2)^{1/2} - P_c + 2kP_c}{2\pi(1 - K)} \quad (5)$$

where Θ is a constant which is a combination of all fixed parameters in Equations (2)–(4).

The solute Péclet number can be expressed as [13]:

$$P_c = \frac{\lambda V}{2D} \quad (6)$$

As the pressure increased, the solute diffusion coefficient decreased exponentially, so the solute Péclet number increased, $P_c \gg 2\pi$ under high pressure. Equation (5) is simplified as follows:

$$\lambda = \Theta \frac{k}{2\pi(1 - K)} \quad (7)$$

The effect of pressure on the solute distribution coefficient can be calculated by Refs. [31–33]:

$$k_p = K \left(1 + \frac{\Delta V_m^B \Delta P}{RT_m} \right) \quad (8)$$

where subscript m represents melting, ΔV_m^B (m^3/mol) is the volume change of component B, ΔP (Pa) is the change in pressure.

By inserting Equation (8) into Equation (7), Equation (7) is obtained as:

$$\lambda = \Theta \frac{k \left(1 + \frac{\Delta V_m^B \Delta P}{RT_m} \right)}{2\pi \left[1 - K \left(1 + \frac{\Delta V_m^B \Delta P}{RT_m} \right) \right]} \quad (9)$$

Equation (9) reflected the relationship between pressure and eutectic spacing. According to Equation (9), the result of calculation for Al-20Si alloy is shown in Figure 6. The calculated results were consistent with the variation pattern of eutectic spacing of the Al-20Si alloy observed in Figure 2. The increase in solidification pressure decreased the eutectic spacing. It can be seen from Figure 6 that the calculated results agree with the results for atmospheric pressure and 1 GPa [28].

It can be seen from Equation (9) that the eutectic spacing under the effect of high pressure depended on the change of the molar volume of the solute phase in the binary alloy during the liquid-solid phase transition. For the Al-20Si alloy, the molar volume of the Si phase becomes larger during the transition from liquid to solid ($\Delta V_{Si}^m = -1.122 \text{ cm}^3/\text{mol}$ [34]). The k_p and λ decreased with increasing pressure. When the volume of the solute phase in the alloy decreased during the transition from liquid to solid, the variation of k_p and λ with pressure was opposite to the above trend. Therefore, once the trend of the molar volume of the solute phase in the alloy during the transition from liquid to solid was determined, the trend of the effect of pressure on the average eutectic spacing could be predicted. This equation was applicable to the condition that the eutectic phase grew in lamellar form.

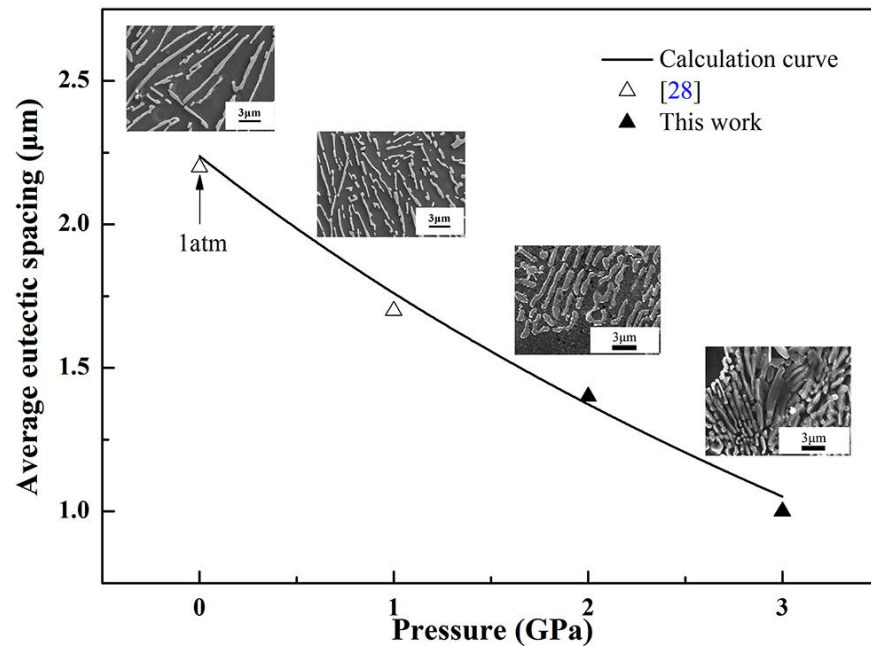


Figure 6. Relationship between pressure and eutectic spacing in Al-20Si alloys solidified under different pressures.

4. Conclusions

The microstructure of the Si phase of the Al-20Si alloy under high pressure was investigated. Then, a mathematical model was developed to analyze the trend of eutectic spacing of Al-Si alloy under the effect of pressure. The results are obtained as follows:

(1) The morphology of Si phase transformed (bulk → short rod → long needle) with the increase of superheat temperature under high pressure. At a pressure of 3 GPa and a superheating temperature of 100 K, a microstructure with a uniform distribution of fine Si phases on the α -Al matrix was obtained in the Al-20Si alloy.

(2) The lamellar Al-Si eutectics appeared at 2 GPa and superheat temperatures of 70–150 K, and at 3 GPa and superheat temperatures of 140–200 K. With the increase of pressure from 2 GPa to 3 GPa, the average spacing of lamellar Al-Si eutectics decreased from 1.2–1.6 μm to 0.9–1.1 μm .

(3) In binary alloys, the effect of pressure on the eutectic spacing is related to the volume change of the solute phase from liquid to solid. When the volume change of the solute phase from liquid to solid is negative, the lamellar eutectic spacing decreases with increasing pressure. When it is positive, the eutectic spacing increases with increasing pressure.

Author Contributions: Conceptualization, R.Z. and C.Z.; methodology, R.Z.; formal analysis, R.Z., C.Z. and Z.W.; investigation, R.Z. and H.W.; resources, Z.W.; data curation, R.Z. and Z.W.; writing—original draft preparation, R.Z. and C.Z.; writing—review and editing, R.Z., Z.W. and H.W. All authors have read and agreed to the published version of the manuscript.

Funding: This work was supported by the National Natural Science Foundation of China [Nos. 51774105] and the “Head Goose” team project [XNAUEA5640208420].

Data Availability Statement: All data and models during the study appear in the submitted article.

Conflicts of Interest: The authors declare no conflict of interest.

References

1. Mostafa, A.; Adaileh, W.; Awad, A.; Kilani, A. Mechanical Properties of Commercial Purity Aluminum Modified by Zirconium Micro-Additives. *Crystals* **2021**, *11*, 270. [[CrossRef](#)]
2. MacLeod, S.; Errandonea, D.; Cox, G.A.; Cynn, H.; Daisenberger, D.; Finnegan, S.; McMahon, M.; Munro, K.; Popescu, C.; Storm, C. The phase diagram of Ti-6Al-4V at high-pressures and high-temperatures. *J. Phys. Condens. Matter* **2021**, *33*, 154001. [[CrossRef](#)] [[PubMed](#)]
3. Smith, D.; Joris, O.P.J.; Sankaran, A.; Weekes, H.E.; Bull, D.J.; Prior, T.J.; Dye, D.; Errandonea, D.; Proctor, J.E. On the high-pressure phase stability and elastic properties of β -titanium alloys. *J. Phys. Condens. Matter* **2017**, *29*, 155401. [[CrossRef](#)] [[PubMed](#)]
4. Thompson, C.V.; Spaepen, F. Homogeneous crystal nucleation in binary metallic melts. *Acta Metall.* **1983**, *31*, 2021–2027. [[CrossRef](#)]
5. Ishihara, K.; Maeda, M.; Shingu, P. The nucleation of metastable phases from undercooled liquids. *Acta Metall.* **1985**, *33*, 2113–2117. [[CrossRef](#)]
6. Cantor, B.; Doherty, R. Heterogeneous nucleation in solidifying alloys. *Acta Metall.* **1979**, *27*, 33–46. [[CrossRef](#)]
7. Tiller, W.; Jackson, K.; Rutter, J.; Chalmers, B. The redistribution of solute atoms during the solidification of metals. *Acta Metall.* **1953**, *1*, 428–437. [[CrossRef](#)]
8. Mullins, W.W.; Sekerka, R.F. Morphological stability of a particle growing by diffusion or heat flow. *J. Appl. Phys.* **1963**, *34*, 323–329. [[CrossRef](#)]
9. Mullins, W.W.; Sekerka, R.F. Stability of a planar interface during solidification of a dilute binary alloy. *J. Appl. Phys.* **1964**, *35*, 444–451. [[CrossRef](#)]
10. Sekerka, R.F. A Stability function for explicit evaluation of the Mullins-Sekerka Interface Stability Criterion. *J. Appl. Phys.* **1965**, *36*, 264–268. [[CrossRef](#)]
11. Sekerka, R.F. Morphological stability. *J. Cryst. Growth* **1968**, *3–4*, 71–81. [[CrossRef](#)]
12. Trivedi, R.; Kurz, W. Morphological stability of a planar interface under rapid solidification conditions. *Acta Metall.* **1986**, *34*, 1663–1670. [[CrossRef](#)]
13. Kurz, W.; Fisher, D.J. *Fundamentals of Solidification*, 4th ed.; Trans Tech Publications LTD: Zurich, Switzerland, 1986.
14. Trivedi, R.; Magnin, P.; Kurz, W. Theory of eutectic growth under rapid solidification conditions. *Acta Metall.* **1987**, *35*, 971–980. [[CrossRef](#)]
15. Trivedi, R. The role of interfacial free energy and interface Kinetics during the growth of precipitate plates and needles. *Metall. Mater. Trans. B* **1970**, *1*, 921–927.
16. Lipton, J.; Kurz, W.; Trivedi, R. Rapid dendrite growth in undercooled alloys. *Acta Metall.* **1987**, *35*, 957–964. [[CrossRef](#)]
17. Wei, Z.J.; Wang, Z.L.; Wang, H.W.; Cao, L. Evolution of microstructures and phases of Al-Mg alloy under 4GPa high pressure. *J. Mater. Sci.* **2007**, *42*, 7123–7128. [[CrossRef](#)]
18. Xu, R. The effect of high pressure on solidification microstructure of Al-Ni-Y alloy. *Mater. Lett.* **2005**, *59*, 2818–2820. [[CrossRef](#)]
19. Jie, J.; Zou, C.; Brosh, E.; Wang, H.; Wei, Z.; Li, T. Microstructure and mechanical properties of an Al-Mg alloy solidified under high pressures. *J. Alloys Compd.* **2013**, *578*, 394–404. [[CrossRef](#)]
20. Jie, J.; Wang, H.; Zou, C.; Wei, Z.; Li, T. Precipitation in Al-Mg solid solution prepared by solidification under high pressure. *Mater. Charact.* **2014**, *87*, 19–26. [[CrossRef](#)]
21. Zhang, R.; Zou, C.M.; Wei, Z.J.; Wang, H.W.; Liu, C. Interconnected SiC-Si network reinforced Al-20Si composites fabricated by high pressure solidification. *Ceram. Int.* **2021**, *47*, 3597–3602. [[CrossRef](#)]
22. Liu, X.; Ma, P.; Jia, Y.D.; Wei, Z.J.; Suo, C.J.; Ji, P.C.; Shi, X.R.; Yu, Z.S.; Prashanth, K.G. Solidification of Al-xCu alloy under high pressures. *J. Mater. Res. Technol.* **2020**, *9*, 2983–2991. [[CrossRef](#)]
23. Zhang, R.; Zou, C.M.; Wei, Z.J.; Wang, H.W.; Ran, Z.; Fang, N. Effects of high pressure and superheat temperature on microstructure evolution of Al-20Si alloy. *J. Mater. Res. Technol.* **2020**, *9*, 11622–11628. [[CrossRef](#)]
24. Ma, P.; Wei, Z.; Jia, Y.; Zou, C.; Scudino, S.; Prashanth, K.; Yu, Z.; Yang, S.; Li, C.; Eckert, J. Effect of high pressure solidification on tensile properties and strengthening mechanisms of Al-20Si. *J. Alloys Compd.* **2016**, *688*, 88–93. [[CrossRef](#)]
25. Wang, X.; Dong, D.; Zhu, D.; Wang, H.; Wei, Z. The Microstructure Evolution and Mass Transfer in Mushy Zone during High-Pressure Solidifying Hypoeutectic Al-Ni Alloy. *Appl. Sci.* **2020**, *10*, 7206. [[CrossRef](#)]
26. Zhang, R.; Zou, C.M.; Wei, Z.J.; Wang, H.W. In situ formation of SiC in Al-40Si alloy during high-pressure solidification. *Ceram. Int.* **2021**. [[CrossRef](#)]
27. Batashef, A.E. *Crystallization of Metals and Alloys under Pressure*, 1st ed.; Moscow Metallurgy: Moscow, Russia, 1977.
28. Ma, P.; Zou, C.; Wang, H.; Scudino, S.; Fu, B.; Wei, Z.; Kühn, U.; Eckert, J. Effects of high pressure and SiC content on microstructure and precipitation Kinetics of Al-20Si alloy. *J. Alloys Compd.* **2014**, *586*, 639–644. [[CrossRef](#)]
29. Yu, X.F.; Zhang, G.Z.; Wang, X.Y.; Gao, Y.Y.; Jia, G.L.; Hao, Z.Y. Non-equilibrium microstructure of hyper-eutectic Al-Si alloy solidified under superhigh pressure. *J. Mater. Sci.* **1999**, *34*, 4149–4152. [[CrossRef](#)]
30. Jackson, K.; Hunt, J. Lamellar and rod eutectic growth. In *Dynamics of Curved Fronts*; Pelcé, P., Ed.; Academic Press: San Diego, CA, USA, 1988.
31. Koutsoyiannis, D. Clausius-Clapeyron equation and saturation vapour pressure: Simple theory reconciled with practice. *Eur. J. Phys.* **2012**, *33*, 295–305. [[CrossRef](#)]
32. Hu, H.Q. *Fundamentals of Metal Solidification*; China Machine Press: Beijing, China, 1999; p. 36. (In Chinese)

-
33. Huang, X.; Han, Z.; Liu, B. Study on the effect of pressure on the equilibrium and stability of the solid-liquid interface in solidification of binary alloys. *Sci. China Technol. Sci.* **2011**, *54*, 479–483. [[CrossRef](#)]
 34. Hallstedt, B. Molar volumes of Al, Li, Mg and Si. *Calphad* **2007**, *31*, 292–302. [[CrossRef](#)]